Extreme Mechanics Letters 84 (2026) 102466

Contents lists available at ScienceDirect

Extreme Mechanics Letters

journal homepage: www.elsevier.com/locate/eml

Diffusion and release of molecules in swelling polymer networks

Tsz Hung Wong [1], Jie Ma [1], Alexander Sherburne, Shaoting Lin [*]

Department of Mechanical Engineering, Michigan State University, East Lansing, MI, USA

ARTICLE INFO

Keywords:
Molecule diffusion
Swelling hydrogel
Mechano-diffusion
Molecule release

ABSTRACT

Molecular diffusion within swelling polymer networks critically controls fundamental processes across biological systems and engineering applications. Existing studies typically model molecule diffusivity as either a constant or as a polymer-concentration-dependent variable following non-Fickian transport, which remain largely phenomenological. Here, we use experiments and theory to investigate molecule diffusion and release in crosslinked polymer networks under swelling. Our fluorescent recovery after photobleaching experiments reveal an intriguing size-dependent diffusion-swelling relationship: molecule diffusivity exhibits a concave dependence on swelling ratio for small molecules, and a convex-to-concave transition for large molecules as the polymer network swells. Our molecule release experiments further demonstrate a consistent size-dependent release–swelling relationship. We analyze this transition using a mechano-diffusion theory that establishes the relationship between molecule diffusivity and swelling-induced deformation of the polymer network. Monte Carlo simulations incorporating this diffusion-swelling transition further predict the release of molecules from swelling polymer networks, agreeing well with experimental observations. This work not only establishes a theoretical framework for molecule diffusion and release in swelling polymer networks, but also offers insights into biological processes involving molecule diffusion and release.

1. Introduction

The diffusion and release of molecules from swelling polymer networks, such as hydrogels, is a fundamental transport phenomenon with broad relevance to therapeutic delivery [1–5], sustainable agriculture [6,7], and emerging soft material technologies [8–12]. Unlike diffusion in liquid media, molecular transport within swellable polymer networks deviates from the Stokes–Einstein relationship, as it is strongly governed by interactions between diffusing molecules and polymer matrix [13,14], with network architecture such as crosslink density and mesh size playing central roles [15]. Upon exposure to solvent-rich environments, swellable polymer matrices absorb solvent and undergo network expansion [16], leading to geometric reconstruction that modifies the constraints experienced by diffusing molecules and can redirect their diffusion pathways [17]. Despite its importance, a clear understanding of how swelling-driven network reconstruction governs molecular mobility remains elusive; yet this process represents a simple and effective mechanism for modulating molecular transport through polymer networks used as carriers.

Traditional treatments of molecule diffusion and release in swelling polymer networks are largely phenomenological. Early empirical descriptions trace back to the Higuchi model [18,19], which is widely used in drug release kinetics, simply assuming a constant molecule diffusivity while neglecting the swelling of polymer networks. Subsequently, Peppas and co-workers introduced models to describe the transition between Fickian and non-Fickian diffusion in swelling polymer networks, depending on whether molecule diffusion is governed primarily by concentration gradient or by polymer relaxation [20,21]. In particular, the Korsmeyer–Peppas model employs a single power-law expression, with the exponent distinguishing Fickian from non-Fickian kinetics [22], whereas the Peppas–Sahlin model incorporates two terms to decouple the contributions of Fickian diffusion and anomalous transport arising from polymer relaxation and network swelling [23]. Although distinguishing between Fickian and non-Fickian diffusion captures the role of swelling at the phenomenological level, it does not elucidate how swelling-induced network expansion and chain straightening mechanistically regulates molecule diffusion and release.

In this work, we combine experiments and theory to systematically investigate the diffusion and release of molecules in swelling polymer networks, involving network-architecture reconfiguration and chain-

* Corresponding author.
E-mail address: linshaot@msu.edu (S. Lin).
[1] These authors contribute equally.

https://doi.org/10.1016/j.eml.2026.102466
Received 9 January 2026; Received in revised form 28 February 2026; Accepted 1 March 2026
Available online 5 March 2026
2352-4316/© 2026 Elsevier Ltd. All rights are reserved, including those for text and data mining, AI training, and similar technologies.

energy modulation. We identify three characteristic regimes as a polymer network evolves from an initially as-prepared state, to a partially swollen state, ultimately to a fully swollen state. These regimes determine the transition in molecule diffusion from complete trapping, to hopping diffusion, to finally obstructed diffusion. We first conduct fluorescence recovery after photobleaching (FRAP) measurements to quantify the diffusivity of molecules with different sizes in hydrogel at controlled swelling ratios. Our FRAP measurements reveal an intriguing size-dependent diffusion-swelling relationship: the diffusivity of small molecules exhibits a concave dependence on swelling ratio, whereas that of large molecules shows a convex dependence at the early swelling stage and then displays a convex-to-concave transition as swelling progresses. To rationalize these observations, we use a mechano-diffusion theory that links molecule diffusivity to swelling-induced deformation of the polymer network. Beyond diffusivity, we conduct molecule release experiments in swelling hydrogels, and the released molecule concentration aligns with the same trend. In parallel, we conduct Monte Carlo simulations that incorporate the diffusion-swelling transition to capture molecule release from swelling polymer networks, achieving quantitative agreement with experimental measurements. The combined experimental and theoretical insights provide a predictive basis for designing swelling-responsive polymer systems with tunable release behaviors across biomedical, environmental, and materials applications.

2. Working principle of molecule diffusion and release in swelling polymer networks

The swelling-induced transition in molecular diffusion behavior can be understood as a continuous crossover between energy-governed and geometry-governed transport regimes, determined by the evolving relationship between molecular size and polymer network mesh size. As illustrated in Fig. 1a, in an as-prepared hydrogel, the hydrodynamic diameter of the diffusing molecules (d) is comparable to or slightly exceeds the polymer mesh size (ξ, defined as the average spacing between adjacent crosslinks). In this state, molecules are transiently confined within polymer cages formed by surrounding chains [24–26]. Molecular transport occurs via hopping diffusion, as proposed by Cai et al. [27], in which migration between adjacent cages requires overcoming local energy barriers imposed by entangled polymer segments, thereby enabling hopping between neighboring cages [28] (Fig. 1a, left). Upon swelling, water uptake dilates the polymer network and increases the mesh size, relaxing chain confinement. Consequently, molecular transport transitions from an energy-barrier-limited hopping regime to a steric-obstruction-controlled diffusion regime. When the mesh size exceeds the molecular dimension ($\xi > d$), the classical obstruction model applies (Fig. 1a, right). From a single-cage perspective (Fig. 1b), swelling reduces the degree of polymer chain deformation required for molecule penetration, thereby continuously lowering the associated elastic energy barrier until cage deformation becomes unnecessary. This continuous crossover from energy-barrier-limited hopping diffusion to geometry-controlled obstructed diffusion constitutes the central concept of the proposed transition model, which unifies these two diffusion mechanisms within a single framework.

3. Experimental results

3.1. Molecule diffusion experiments

To characterize molecular diffusion in swelling hydrogels, FITC–dextran was selected as a model probe owing to its well-defined molecular size, strong fluorescence, and compatibility with fluorescence recovery after photobleaching (FRAP). FITC–dextran is first homogeneously mixed into the polyacrylamide (PAAm) hydrogel precursor solution prior to gelation. After polymerization, the hydrogels were immersed in DI water containing the same concentration of FITC–dextran to allow swelling while maintaining the equilibrium concentration (Fig. 2a). The dimensional evolution of PAAm hydrogels is monitored during swelling. The hydrogel continuously swells within the first 200 min and reaches equilibrium at approximately 1100 min, with a swelling ratio in length of approximately 2 (Fig. 2b). Correspondingly, the inferred polymer mesh size increases from approximately 13 nm to 26 nm during swelling (Fig. 2c, Eq. 7). Hydrogels at different swelling stages are then subjected to FRAP measurements. In a typical FRAP experiment, a high-intensity laser pulse is used to photobleach a small circular region within the hydrogel, effectively extinguishing the fluorescence of FITC–dextran in the selected area. Fluorescent molecules from the surrounding unbleached regions subsequently diffuse into the bleached zone (Fig. 2d). By continuously

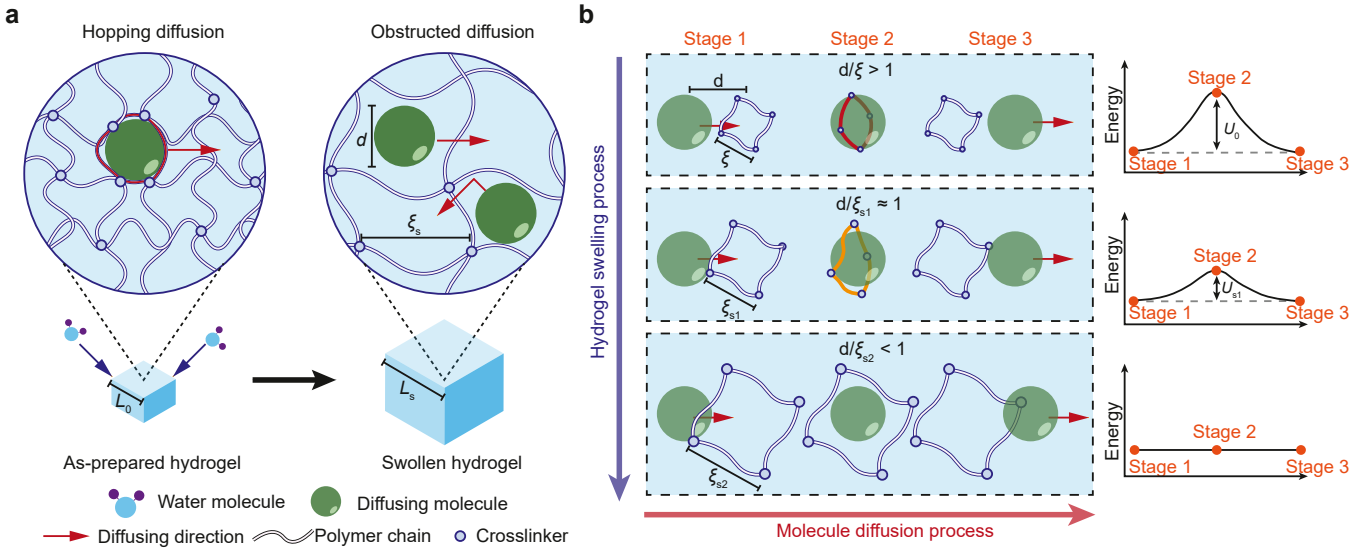


Fig. 1. Transition of molecular diffusion from hopping diffusion to obstructed diffusion during hydrogel swelling. (a) Schematic illustration of a large molecule initially entrapped within a polymer network and undergoing hopping diffusion. As hydrogel swells and the polymer network expands, the molecule becomes effectively smaller relative to the mesh size and transitions to obstructed diffusion. (b) Schematic illustrations of a molecule penetrating a polymer cage at different swelling stages (where $\xi_{s2} > \xi_{s1}$, indicating an increased mesh size upon swelling), highlighting the deformation of the polymer network and the corresponding strain energy during the penetration process.

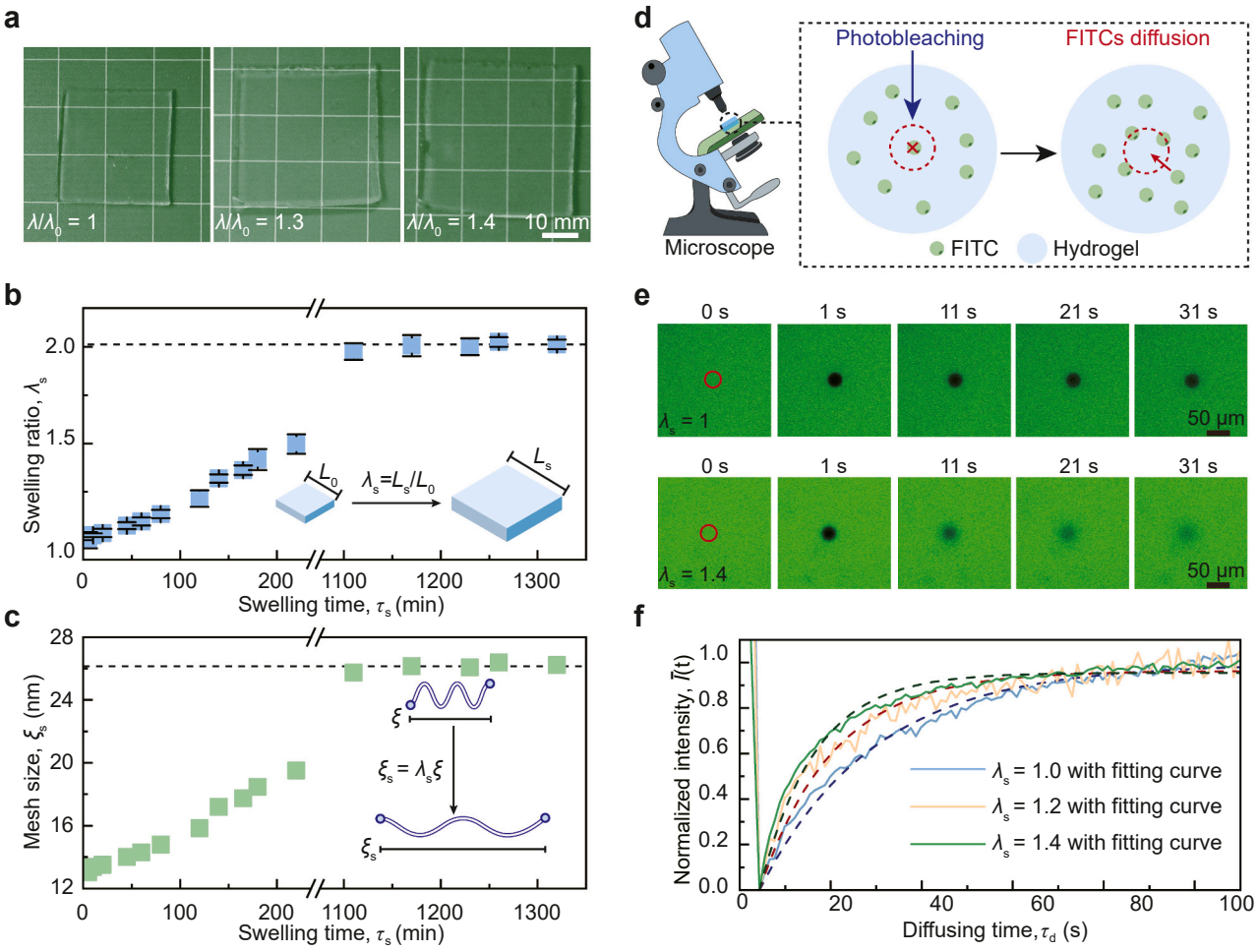


Fig. 2. Characterization of hydrogel swelling and molecule diffusion. (a) Optical images of the hydrogel at various ratios of swelling. (b) Hydrogel swelling ratio as a function of swelling time. (c) Corresponding calculated mesh size versus swelling time. (d) Schematic illustration of the fluorescence recovery after photobleaching (FRAP) experiment. (e) Optical images showing the bleached area of hydrogels loaded with FITC–dextran in both as-prepared and swollen states, along with the fluorescence recovery process. (f) Normalized fluorescence intensity versus diffusion time for FRAP results of hydrogels with varying swelling ratios. Values in (b) represent mean ± SD (n = 3).

monitoring the fluorescence recovery over time, the effective diffusivity of FITC–dextran within the hydrogel is quantitatively extracted from the recovery profiles. As shown in Fig. 2e, representative FRAP images at different time points illustrate the fluorescence recovery process in both pristine and swollen hydrogels. In both cases, a circular region is photobleached at $t = 1$ s. By $t = 31$ s, the fluorescence intensity within the bleached region of the swollen hydrogel recovers more rapidly than that of the as-prepared hydrogel. The corresponding normalized fluorescence recovery curves in Fig. 2f further confirm this trend. With increasing swelling, the fluorescence recovery rate increases, indicating enhanced FITC mobility and higher molecular diffusivity. The diffusivity is quantitatively extracted from the recovery profiles using the Soumpasis equation [29,30]. These results demonstrate that FRAP provides an effective platform for quantifying molecular diffusivity in swelling hydrogels.

3.2. Molecule diffusion results

We select three FITC–dextran samples with different molecule sizes—40 kDa, 150 kDa, and 250 kDa—corresponding to hydrodynamic diameter–to–mesh size ratios (d/ξ) of 0.6, 1.2, and 1.6, respectively (Appendix B). We compile the normalized diffusivity of each FITC–dextran across hydrogels at different swelling ratios, where the diffusivity is normalized by its value in the as-prepared hydrogel. As shown in Fig. A1, the normalized diffusivity of 40 kDa FITC–dextran ($d/\xi = 0.6$) increases monotonically with hydrogel swelling and is expected to gradually approach a steady-state value. This overall trend exhibits an approximately concave dependence on swelling ratio, indicating a progressively diminishing enhancement in diffusivity. Notably, for larger FITC–dextran molecules with $d/\xi > 1$ (150 kDa and 250 kDa; Fig. 3a,b), the normalized diffusivity increases slowly only in the as-prepared hydrogel and during the early stages of swelling. As the swelling proceeds and the swelling ratio approaches a critical threshold, the normalized diffusivity exhibits a pronounced acceleration, forming a convex segment in the curve. With further swelling, the rate of increase slows down and eventually reaches a plateau, giving rise to a concave regime at high swelling ratios. Overall, for molecules whose size exceeds the polymer mesh size ($d/\xi > 1$), the normalized diffusivity displays a characteristic convex-to-concave transition with increasing swelling: an initial slow increase, followed by a rapid rise, and finally a gradual saturation. This transition is more pronounced for the 250 kDa FITC–dextran.

3.3. Molecule release experiments

In addition to the FRAP experiments, a complementary release assay is performed to investigate the release behavior of molecules in swelling hydrogels. FITC–dextran–loaded hydrogels are immersed in an aqueous

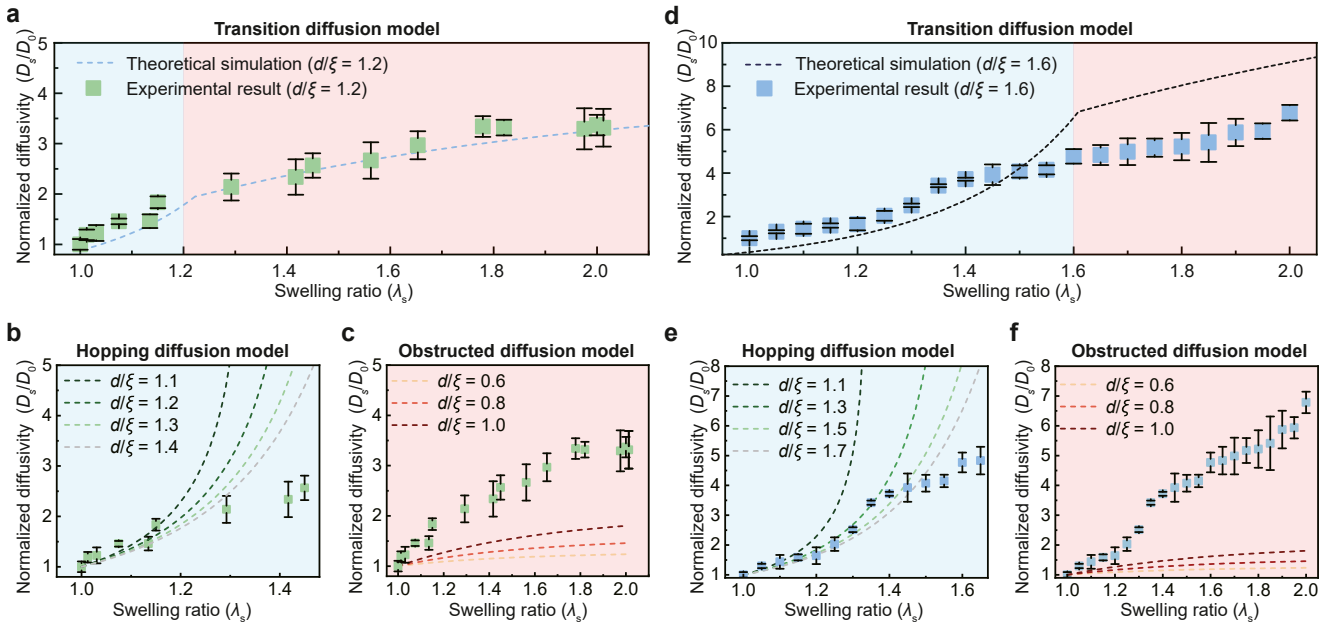


Fig. 3. Characterization of FRAP results for FITC–dextran–loaded hydrogels with varying swelling ratios. Normalized diffusivity ratios of 150 kDa FITC–dextran ($d/\xi = 1.2$) in hydrogels with different swelling ratios, fitted using (a) the transition diffusion model, (b) the hopping diffusion model, and (c) the obstructed diffusion model. Normalized diffusivity ratios of 250 kDa FITC–dextran ($d/\xi = 1.6$) in hydrogels with different swelling ratios, fitted using (d) the transition diffusion model, (e) the hopping diffusion model, and (f) the obstructed diffusion model. All values represent mean ± SD (n = 6, three bleached spots per gel, two independently prepared hydrogels).

environment to allow free swelling, and the concentration of FITC–dextran released into the surrounding solution is monitored over time. The temporal evolution of the released FITC–dextran concentration is used to characterize the diffusion-governed release behavior in the swelling hydrogel (Fig. 4a). The same FITC–dextran species as those used in the FRAP experiments are employed to ensure consistency. Prior to the release study, calibration correlating fluorescence intensity with FITC–dextran concentration is established (Fig. A2). All three FITC–dextran samples exhibit stable linear fluorescence–concentration relationships, enabling reliable quantitative analysis of FITC–dextran

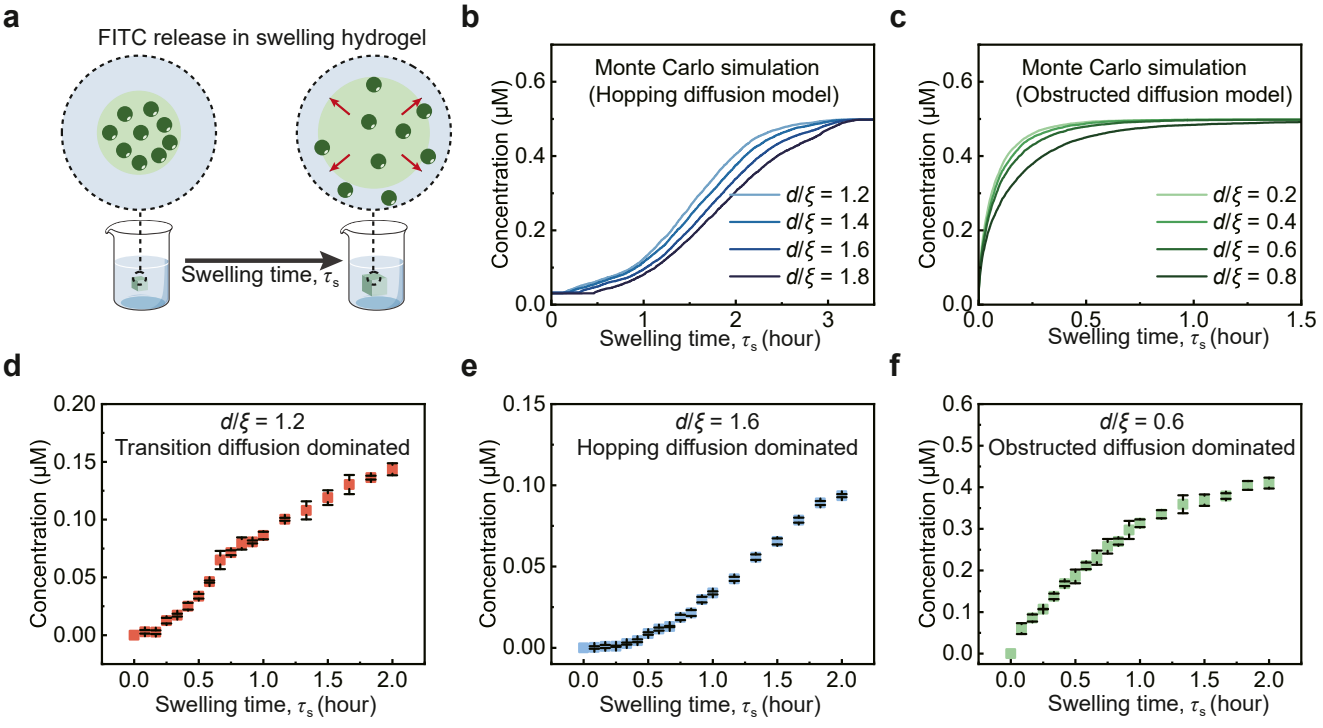


Fig. 4. Characterization of the release profiles of swelling hydrogels. (a) Schematic illustration of FITC–dextran release from a hydrogel during swelling. Monte Carlo simulations of the release profiles based on (b) the hopping diffusion model and (c) the obstructed diffusion model. Temporal evolution of FITC–dextran concentration in the surrounding water for (d) 150 kDa FITC–dextran ($d/\xi = 1.2$), (e) 250 kDa FITC–dextran ($d/\xi = 1.6$), and (f) 40 kDa FITC–dextran ($d/\xi = 0.6$). Values in (d, e, f) represent mean ± SD (n = 3).

concentration in the external solution.

3.4. Molecule release results

From the concentration–time profiles of FITC–dextran permeation, the smallest dextran (40 kDa, $d/\xi = 0.6$) exhibits a classic monotonic increase in the concentration in deionized (DI) water followed by a gradual slowdown toward a plateau (Fig. 4f). The concentration reaches a plateau at approximately 0.4 μM within the observation window. In contrast, the larger dextrans (150 kDa, $d/\xi = 1.2$; 250 kDa, $d/\xi = 1.6$) display a distinct early-stage behavior (Fig. 4d,e). Consistent with the FRAP observations for larger molecules, the concentration in DI water increases only slowly at the onset of swelling, followed by a rapid rise that yields a convex segment in the early-time profile (approximately within the first ~0.7 h for 150 kDa and ~1 h for 250 kDa). With continued swelling, the rate of increase progressively diminishes and the profiles transition into a concave shape, ultimately approaching a plateau similar in overall trend to that of the 40 kDa dextran. Taken together, these results indicate that for larger molecules ($d/\xi > 1$), the release profile during swelling undergoes a transient convex-to-concave transition. Notably, this transition is confined to the early swelling period and is short-lived. This feature is therefore easily overlooked when considering only long-duration release curves, which extend beyond 12 h (Fig. A3).

4. Theoretical analysis of size-dependent molecule diffusion in swelling polymer networks

4.1. Theoretical formulation

To analyze the observed transition, we perform a theoretical analysis to rationalize the diffusion and release behavior of molecules in swelling hydrogels. Distinct theoretical frameworks are adopted for small molecules ($d/\xi < 1$) and large molecules ($d/\xi > 1$), based on spatial geometric considerations and energy-based arguments, respectively. All molecules are assumed to be spherical and incompressible.

We start by quantifying the swelling behavior of a hydrogel matrix. The isotropic swelling of hydrogel is assumed to be a uniform three-dimensional expansion. In the undeformed (as-prepared) state, the principal stretch ratios are $\lambda_x = \lambda_y = \lambda_z = 1$. When the hydrogel undergoes free swelling, its swelling ratio λ_s can be defined as

$$\lambda_s = \frac{L_s}{L_0} = \left(\frac{V_s}{V_0}\right)^{\frac{1}{3}} \tag{1}$$

where L_s and L_o denote the linear dimensions of the hydrogel in the swollen and as-prepared states, respectively, and V_s/V_0 represents the volumetric swelling ratio. On the other hand, the mesh size scale with the volumetric swelling ratio as,

$$\xi_s = \xi\left(\frac{V_s}{V_0}\right)^{\frac{1}{3}} \tag{2}$$

where ξ_s and ξ denote the average mesh sizes of the polymer network in the swollen and as-prepared states, respectively. By combining these two equations, we obtain,

$$\frac{L_s}{L_0} = \frac{\xi_s}{\xi} \tag{3}$$

Accordingly, the hydrogel's dimensional changes are used to estimate the corresponding variations in its internal mesh size, which is characterized as $\xi_s = \lambda_s \xi$.

Case I: Small molecules

We adopt the classical obstructed diffusion model for small molecules. In the obstructed diffusion model, the diffusivity (D_0) of spherical molecules, normalized by the diffusivity of immersed solution within the unperturbed hydrogel is expressed as [31],

$$\frac{D_0}{D_{sol}} = \exp\left[-\frac{\pi}{4}\left(\frac{d}{\xi}\right)^2\right] \tag{4}$$

where d is the diameter of the diffusing molecule. Upon swelling, the mesh size of the hydrogel increases, leading to an enhancement in diffusivity. The corresponding diffusivity (D_s) in the swollen hydrogel is given by

$$\frac{D_s}{D_{sol}} = \exp\left[-\frac{\pi}{4}\left(\frac{d}{\lambda_s \xi}\right)^2\right] \tag{5}$$

Diffusivity of spherical molecules in the swollen hydrogel can be normalized by that in the reference state to quantify the impact of swelling on diffusion. By introducing the swelling ratio as a geometric scaling factor, the normalized diffusivity has the expression as

$$\frac{D_s}{D_0} = \exp\left[\frac{\pi}{4}\left(1 - \frac{1}{\lambda_s^2}\right)\left(\frac{d}{\xi}\right)^2\right] \tag{6}$$

Case II: Large molecules

To account for the interaction between large molecules and the surrounding polymer network, the classical eight-chain model is employed. This model represents an isotropic polymer network as eight equivalent polymer chains aligned along the body diagonals of a cubic unit cell. Under mechanical deformation, the eight-chain model describes how macroscopic strain is distributed among individual polymer chains [32]. Within this framework, the undeformed chain length ξ is defined as

$$\xi = \sqrt{N}b \tag{7}$$

Here, b denotes the Kuhn length, and N represents the number of Kuhn-length segments between two adjacent crosslinkers. For the PAAm hydrogel used in all experiments, $b = 0.3$ nm [33], yielding an estimated chain length ξ of approximately 13 nm.

When the hydrogel undergoes swelling, all polymer chains dilate isotropically, such that the stretch ratio of an individual polymer chain $\Lambda = \xi_s/\xi$, which is correlated with the swelling ratio of the polymer λ_s, which can be expressed as

$$\lambda_x = \lambda_y = \lambda_z = \lambda_s \tag{8}$$

The stretch ratio of the polymer chain can be rewritten as

$$\Lambda = \sqrt{\frac{1}{3}(\lambda_x^2 + \lambda_y^2 + \lambda_z^2)} = \lambda_s \tag{9}$$

Thus, the stretch ratio of an individual polymer chain is directly related to the stretch ratio of the swelling polymer network.

To correlate the free energy of an individual polymer chain with its stretch ratio, the ideal chain model is employed. This model accounts for the finite extensibility of a polymer chain with a maximum contour length Nb. According to Langevin statistics, the relationship between the force f and an individual polymer chain and its chain length ξ is given by

$$f = \frac{k_b T}{b}\beta \tag{10}$$

By integrating the above equation, we can obtain the free energy function expressed as [34]

$$W = NkT\left(\frac{\beta}{\tanh\beta} + \log\frac{\beta}{\sinh\beta}\right) \tag{11}$$

where N is the number of chains of the network per unit volume. The chain force β relates to the stretch Λ as $\beta = L^{-1}\left(\Lambda/\sqrt{N}\right)$ with L^{-1} being the inverse Langevin function defined by $L(x) = \coth(x) - 1/x$.

The energy barrier for a large molecule doing one-step hopping

diffusion in the reference state is the energy difference before and when the molecule is diffusing through the cage, given by

$$U = W(\Lambda_{\mathrm{H}}) - W(\Lambda_{\mathrm{L}}) \tag{12}$$

We first analyze the energy barrier experienced by molecules in the as-prepared hydrogel without swelling. For the polymer cage without molecules, the chain stretch ratio is $\Lambda_{\mathrm{L}} = 1$. In contrast, as the molecule is diffusing through the eight-chain cage, the chain length in the polymer cage with molecules is

$$\xi_H = \sqrt{d^2 + \frac{{c_0}^2}{4}} \tag{13}$$

where $c_0 = 2/\sqrt{3}\xi$ denotes the edge length of the eight-chain cube (Fig. B1a). The corresponding stretch ratio $\Lambda_{\mathrm{H}} = \xi_H/\xi$ can be expressed as

$$\Lambda_{\mathrm{H}} = \sqrt{(\frac{d}{\xi})^2 + \frac{1}{3}} \tag{14}$$

Combining the above equations, the energy barrier for a large molecule to overcome through hopping diffusion in the as-prepared hydrogel is

$$U = W\left(\sqrt{(\frac{d}{\xi})^2 + \frac{1}{3}}\right) - W(1) \tag{15}$$

For large molecules migrating between neighboring polymer cages, molecular transport is governed by the need to overcome the energy barrier described above, and the resulting diffusivity can be evaluated using the hopping diffusion model [27].

$$D \cong \frac{\xi_c^2}{\tau_r}\left(\frac{d}{\xi}\right)^{-1} \exp\left[-\left(\frac{d}{\xi}\right)^2\right] \tag{16}$$

where ξ_c is the correlation length of the network, and τ_r represents the relaxation time of the polymer chains. During a complete hopping step, the molecule has to overcome an energy barrier U, which can be approximated as

$$\frac{U}{kT} \cong \left(\frac{d}{\xi}\right)^2 \tag{17}$$

This equation is introduced as a controlled scaling approximation within the hopping-dominated regime. In the moderate swelling range relevant to this study, it preserves the functional dependence of the hopping barrier on the normalized size ratio and therefore does not alter the predicted convex–concave transition in diffusivity.

The diffusivity of large molecules in the hopping diffusion model can be reformulated by combining Eq. (16) and Eq. (17), yielding

$$D \cong \frac{\xi_c^2}{\tau_r}\left(\sqrt{\frac{U}{kT}}\right)^{-1} \exp\left(-\frac{U}{kT}\right) \tag{18}$$

We next analyze molecular diffusivity in swelling hydrogels, where the polymer mesh size evolves as a function of the swelling ratio. The swelling ratio λ_s is introduced to chain stretch ratios to determine the stretch ratio $\Lambda_{\mathrm{L}}^{\mathrm{s}}$, and $\Lambda_{\mathrm{H}}^{\mathrm{s}}$ (Fig. B1b) which are expressed as

$$\Lambda_{\mathrm{L}}^{\mathrm{s}} = \sqrt{\frac{1}{3}(3\lambda_s^2)} = \lambda_s \tag{19}$$

and

$$\Lambda_{\mathrm{H}}^{\mathrm{s}} = \sqrt{\left(\frac{d}{\xi}\right)^2 + \frac{1}{3}\lambda_s^2} \tag{20}$$

Substituting Eqs. (19) and (20) into Eq. (15) yields the corresponding strain energy U_s at the swelling stage. To quantify the effect of swelling-induced chain elongation on molecular diffusivity, the diffusivity in the swollen hydrogel (D_s) is normalized by that in the as-prepared hydrogel (D_0). The normalized diffusivity is expressed as:

$$\frac{D_s}{D_0} = \sqrt{\frac{U_0}{U_s}}\exp(\frac{U_0 - U_s}{kT}) \tag{21}$$

When the normalized molecule diameter d/ξ is larger than 1, this large molecule is initially confined within the hydrogel network. When $\lambda_s < d/\xi$, the network mesh size remains smaller than the molecular diameter, and molecular transport is therefore governed by the hopping diffusion model. As swelling proceeds and the mesh size increases, a transition occurs at approximately $\lambda_{\mathrm{c}} = d/\xi$, beyond which the molecule becomes relatively small compared to the network, and obstructed diffusion becomes the dominant transport mechanism.

$$\frac{D_s}{D_0} = \begin{cases} \sqrt{\frac{U_0}{U_s}}\exp\left(\frac{U_0 - U_s}{kT}\right), & \text{when } \lambda_s < \lambda_{\mathrm{c}} \\ \exp\left[\frac{\pi}{4}\left(1 - \frac{1}{\lambda_s^2}\right)(\frac{d}{\xi})^2\right], & \text{when } \lambda_s > \lambda_{\mathrm{c}} \end{cases} \tag{22}$$

The eight-chain model employed in this work was originally developed to describe the large-deformation elasticity of rubber-like polymer networks, where the mechanical response is primarily governed by polymer-chain stretching. Although PAAm hydrogels are formed by randomly crosslinked networks containing chain entanglements and structural heterogeneity, the eight-chain representation is not intended as a literal reconstruction of the network architecture. Instead, it provides a physically motivated framework that captures the scaling relationship between macroscopic swelling deformation and chain elastic free energy. Under rubbery and solvent-swollen conditions, large-deformation behavior is typically dominated by entropic chain stretching, making network-based descriptions a reasonable approximation. Importantly, the predicted diffusion-mechanism transition depends primarily on the scaling of elastic energy with swelling ratio rather than on the specific choice of constitutive model. Regarding the sensitivity of the predicted transition to network heterogeneity, PAAm hydrogels inherently exhibit spatial variations in mesh size, and the use of a single mean mesh size therefore represents idealization. Nevertheless, moderate heterogeneity is expected to primarily smooth quantitative variations rather than fundamentally alter the diffusion-mechanism transition. As the transition is governed by the relative size ratio between the particle and the characteristic network scale, its existence is determined by the underlying transport physics rather than small spatial fluctuations. Thus, the mean mesh size approximation captures the dominant features of the regime transition, while more detailed heterogeneous models may refine quantitative predictions.

4.2. Interpretation of experimental results

By combining the proposed transition diffusion model with the FRAP experimental data, the convex-to-concave evolution of normalized diffusivity observed for large molecules during the early stage of hydrogel swelling can be rationalized. As shown in Fig. 3a and d, the transition model (dashed lines) effectively bridges the hopping diffusion regime dominating the early swelling stage (blue shaded region) and the obstructed diffusion regime governing the intermediate-to-late swelling stage (red shaded region). Notably, the transition points of the model occur at swelling ratios close to the corresponding size ratios d/ξ, namely ~1.2 for 150 kDa FITC–dextran and ~1.6 for 250 kDa FITC–dextran. Although the experimental results for 250 kDa FITC–dextran show some deviation from the theoretical curve at high swelling ratios, likely arising from uncertainties in molecular size estimation, the overall trend remains consistent. The resulting theoretical curves exhibit agreement with the FRAP measurements, providing

strong evidence that particle diffusivity in swelling hydrogels is predominantly governed by the interplay between particle size and polymer mesh size.

For comparison, the same datasets are independently fitted using the pure hopping diffusion model (Fig. 3b,e) and the pure obstructed diffusion model (Fig. 3c,f). In both cases, the fitting quality is markedly inferior to that of the transition model. On one hand, the hopping diffusion model systematically overestimates diffusivity enhancement at later stages of swelling. This discrepancy likely arises from the assumption that particles are effectively immobilized in the as-prepared or minimally swollen state, followed by an abrupt recovery of bulk-like diffusivity once hopping becomes possible. Such an assumption leads to order-of-magnitude increases in diffusivity, which are inconsistent with the more gradual diffusivity evolution observed experimentally during swelling. On the other hand, the obstructed diffusion model tends to underestimate diffusivity enhancement at later stages of swelling. Because this model primarily attributes diffusivity changes to variations in polymer mesh size, it predicts a near-proportional relationship between swelling ratio and diffusivity ratio. However, this framework neglects the early-stage confinement of large molecules by polymer chains, where diffusivity is instead dominated by the need to overcome energetic barriers rather than geometric obstruction. As swelling proceeds, the governing mechanism gradually shifts toward mesh size-controlled diffusion, a transition that is inherently absent from the pure obstructed diffusion model. Taken together, these results demonstrate that the transition diffusion model provides a more accurate and physically grounded description of the size-dependent diffusivity evolution of large molecules in swelling hydrogels, enabling improved interpretation and prediction of their transport behavior.

These considerations also help define the class of polymer networks to which the present analysis applies. Molecular transport in elastically crosslinked hydrogels in the rubbery, solvent-swollen state is primarily governed by the relationship between molecular size and polymer network mesh size, as chain mobility is relatively high and stress relaxation is fast compared with the diffusion timescale. Under these conditions, diffusion behavior can be interpreted in terms of geometric confinement and energetic barriers associated with the network structure. Similar behavior is therefore expected in other neutral, elastically crosslinked hydrogels undergoing moderate swelling. By contrast, the present framework is less applicable to polymer networks that swell only minimally, where changes in mesh size may be insufficient to induce transitions between diffusion mechanisms, as well as to glassy or vitrified polymers and highly swollen ionic or superabsorbent hydrogels. In such systems, transport may be dominated by segmental relaxation, strong polymer–solute interactions, or electrostatic effects, and additional physical mechanisms would need to be considered explicitly.

It is worth noting that during swelling, polymer networks develop internal stresses arising from the balance between osmotic pressure and network elasticity. In many theoretical descriptions of swelling polymer networks, molecular diffusivity is treated as an intrinsic material parameter independent of deformation [35]. Within this framework, swelling primarily influences transport kinetics by changing geometric length scales, concentration distributions, and chemical potential gradients. Accordingly, the present study focuses on how swelling-induced evolution of mesh size alters the relative size ratio between diffusing molecules and the network, thereby governing diffusion mechanisms. Possible effects associated with stress-dependent chain mobility are not explicitly modeled and are implicitly reflected in the experimentally measured swelling kinetics used in the analysis.

In addition to geometric confinement and network elasticity, interactions between polymer chains and diffusing molecules may also influence molecular transport. Weak attractive or repulsive polymer–solute interactions can modify the effective energy barrier associated with molecular migration and thereby affect the quantitative value of diffusivity, as discussed in previous studies of hopping transport in polymer networks. In the present PAAm–dextran system, however, the diffusion behavior is primarily governed by geometric confinement and the evolution of the size ratio between the molecule and the polymer mesh size (d/ξ). Polymer–solute interactions may smooth the transition between diffusion regimes or shift its onset but are not expected to alter the existence of the convex-to-concave transition itself, which is fundamentally controlled by the geometric and elastic characteristics of the network. In systems with strong specific interactions, such as charged hydrogels or networks containing binding sites, interaction effects may become dominant and would require explicit incorporation of interaction-dependent energy terms into the transport model.

The diffusion–mechanism transition identified in this work also provides insight into the design of responsive hydrogel-based drug delivery systems. A critical condition emerges when the characteristic polymer mesh size becomes comparable to the molecular size, at which point the dominant transport mechanism and effective molecular mobility change rapidly. This transition provides a physically meaningful guideline for regulating the onset of accelerated release and for controlling burst release behavior by tailoring polymer network mesh size through crosslink density, swelling behavior, or network architecture. Because mesh size can also be modulated by mechanical deformation or other external stimuli, similar principles may be extended to mechanically or stimuli-responsive hydrogels, suggesting that controlling the relative size ratio between diffusing molecules and the evolving polymer network structure represents a general strategy for achieving selective and tunable molecular transport in soft polymer systems.

5. Monte carlo simulations

To further understand molecular release from swelling hydrogels, Monte Carlo simulations are performed to model this process. Monte Carlo simulations capture the overall transport behavior by performing a large number of random diffusion events under prescribed physical rules and analyzing the resulting statistical outcomes. We simulate a diffusion-controlled molecular release process with a time-evolving confined domain. A finite spatial region is predefined to represent the initially confined volume, within which 5000 non-overlapping molecules are uniformly distributed at the start of the simulation. All molecules undergo Brownian motion with random diffusion directions throughout the simulation space. The confined region expands over time according to experimentally measured swelling kinetics, while no explicit polymer chains or network structures are introduced. Instead, the molecular step length is treated as an effective, time-dependent parameter that reflects the experimentally determined swelling behavior and the evolving relationship between molecular size and the characteristic transport length scale, captured through either hopping- or obstructed-diffusion models. Molecules that cross the boundary of the expanding hydrogel region are considered released into the surrounding solution. After release, molecules continue to diffuse in random directions, while experiencing different diffusivities depending on their location. Within the hydrogel, the diffusivity is time-dependent and determined by the instantaneous swelling state, calculated based on either the hopping diffusion model or the obstructed diffusion model. In the surrounding medium, the diffusivity is assumed to be constant at 1.68×10^{-10} m^2s^{-1}, corresponding to the diffusivity of small FITC-dextran in water estimated using the Stokes–Einstein equation [28]. Molecules are allowed to move bidirectionally across the hydrogel–solution interface, so released molecules may re-enter the hydrogel depending on their stochastic trajectories. By tracking the temporal evolution of molecular populations inside and outside the confined region, statistical analysis of the particle trajectories yields the time-dependent release profile and the corresponding evolution of effective molecular diffusivity. In the present Monte Carlo simulations, the experimentally measured swelling kinetics are prescribed to represent the time evolution of the polymer network mesh size and to examine how diffusion–mechanism transitions at different size ratios influence molecular release behavior. The purpose of these simulations

is to elucidate the overall trends in the release curves arising from diffusion–mechanism transitions, rather than to quantitatively predict release kinetics.

On one hand, for large molecules ($d/\xi > 1$) (Fig. 4b), the simulated release profiles exhibit a characteristic convex-to-concave transition, consistent with the evolution of diffusivity during swelling. Moreover, as molecular size increases, the transition point shifts to later times, indicating that a larger polymer mesh size is required for the diffusion mechanism to transition from hopping diffusion to obstructed diffusion. On the other hand, for small molecules ($d/\xi < 1$) (Fig. 4**c**), the release profiles display a typical concave shape, with the concentration gradually increasing and asymptotically approaching a steady state. Larger molecules reach this steady state more slowly.

To further elucidate molecular release from swelling hydrogels, Monte Carlo simulations are performed under the same experimental parameters to provide a visualized representation of the diffusion process (Fig. 5a). For large molecules governed by the hopping diffusion model, all molecules (green) are initially confined within the hydrogel at the onset of swelling (diffusing time, $\tau_d = 0$ h). As swelling proceeds, the hydrogel expands, while large molecules remain largely confined within the network at the initial swelling stages, exhibiting slow transport with a characteristic diffusion timescale of $\tau_d = 3$ h. At $\tau_d = 6$ h, a fraction of the molecules begins to escape into the surrounding aqueous phase, while a significant number remains inside the gel.

The corresponding theoretical diffusivity is illustrated in Fig. 5b and the simulated molecular concentration in the surrounding water (Fig. 5c) exhibits a characteristic convex-to-concave evolution, consistent with the transition in diffusion behavior during swelling. In contrast, when large molecules are replaced by small molecules, the dominant diffusion mode shifts to obstructed diffusion. As shown in Fig. 5d, all molecules are initially confined within the hydrogel; however, by $\tau_d = 3$ h, a substantial fraction of the molecules has already diffused into the surrounding water. By $\tau_d = 6$ h, noticeably more molecules are released compared to the hopping diffusion case. Correspondingly, both the theoretical diffusivity (Fig. 5e) and the simulated concentration in the surrounding water (Fig. 5f) display concave-shaped profiles, in agreement with the FRAP measurements and macroscopic release experiments. It is worth noting that although bidirectional transport across the hydrogel–water interface is permitted in the simulation, the orders-of-magnitude difference in diffusivity between the hydrogel and water results in rapid dispersion of particles into the surrounding solution once they exit the gel. Although minor discrepancies in absolute timescales are observed between the Monte Carlo simulations and experiments, arising from an effective transport description rather than a fully resolved microscopic interaction model, the simulations capture the overall evolution of diffusivity and molecular release profiles. These results highlight the ability of the Monte Carlo approach to reproduce size-dependent release behavior driven by swelling-induced transport transitions.

6. Conclusion remarks

In conclusion, this work provides a mechanistic understanding of molecular diffusion and release in swelling polymer networks by explicitly linking transport behavior to swelling-induced network reconfiguration. Through a combination of FRAP measurements, release experiments, theoretical modeling, and Monte Carlo simulations, we demonstrate that molecular diffusivity evolves in a size-dependent manner governed by the interplay between molecule size and polymer mesh size. Small molecules exhibit a monotonic concave dependence of diffusivity and release on swelling, whereas large molecules undergo a distinct convex-to-concave transition associated with a shift from hopping diffusion to obstructed diffusion. The proposed mechano-diffusion framework captures this transition by accounting for both geometric and energetic effects arising from network deformation during swelling. Monte Carlo simulations incorporating this diffusion–swelling coupling successfully reproduce the experimentally observed release profiles, further validating the framework. Together, these results move beyond phenomenological descriptions of diffusion in swelling polymer networks and establish a predictive basis for understanding and controlling molecular transport. This insight offers practical guidelines for the design of swelling-responsive polymer systems with tunable diffusion and release properties across biomedical, environmental, and soft material applications.

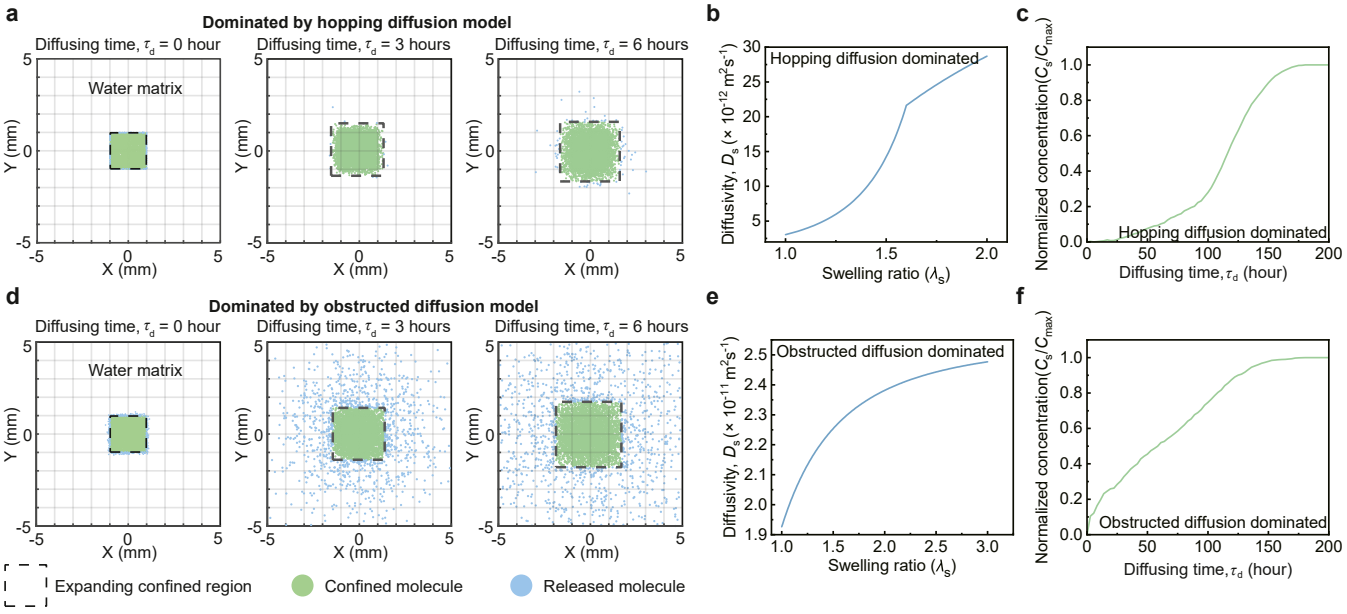


Fig. 5. Monte Carlo simulations of FITC molecule release from an expanding confined region. (a–c) Hopping diffusion model: (a) Visualization of molecule release into the surrounding environment as the confined region expand; (b) Diffusivity versus hydrogel swelling ratio according to hopping diffusion model; (c) corresponding temporal changes in FITC concentration. (d–f) Obstructed diffusion model: (d) Visualization of FITC molecule diffusion into the surrounding environment during expansion of the confined region; (e) Diffusivity versus hydrogel swelling ratio according to obstructed diffusion model; (f) corresponding temporal evolution of FITC concentration.

CRediT authorship contribution statement

Tsz Hung Wong: Writing – review & editing, Writing – original draft, Visualization, Validation, Software, Methodology, Formal analysis, Data curation, Conceptualization. **Jie Ma:** Writing – review & editing, Validation, Methodology, Investigation, Formal analysis, Conceptualization. **Alexander Sherburne:** Investigation, Formal analysis, Data curation. **Shaoting Lin:** Writing – review & editing, Supervision, Project administration, Methodology, Investigation, Funding acquisition, Formal analysis, Conceptualization.

Declaration of Competing Interest

The authors declare that they have no known competing financial interests or personal relationships that could have appeared to influence the work reported in this paper.

Acknowledgement

This work is supported by National Science Foundation grant CBET 2320716 and CMMI 2338747.

Appendix A. Synthesis and Characterizations

Material and method

All materials were purchased from Sigma-Aldrich unless otherwise specified. For hydrogel synthesis, acrylamide (AAm), *N,N′*-methylenebisacrylamide (MBAA), ammonium persulfate (APS), and tetramethylethylenediamine (TEMED) were used. Fluorescein isothiocyanate (FITC)–dextran with molecular weights of 40, 150, and 250 kDa was employed.

Synthesis of PAAm hydrogel

Polyacrylamide (PAAm) hydrogels were prepared by dissolving 2 g of AAm, 0.5 mL of MBAA solution (0.23 wt%), 400 μL of APS solution (10 wt %), and 10 μL of TEMED in 10 mL of deionized (DI) water. The precursor solution was thoroughly mixed, degassed for 30 s, and subsequently vacuum-degassed for 5 min to remove residual air bubbles. The resulting solution was cast into acrylic molds (2 cm × 2 cm × 1.5 mm) and covered with quartz glass prior to polymerization. For FRAP experiments, FITC–dextran was incorporated into the precursor solution at a concentration of 20 mg mL^{-1} . The mixtures were cast into acrylic molds (1 cm × 1 cm × 1.5 mm) and covered with quartz glass. For release experiments, FITC–dextran of different molecular weights was added to separate precursor solutions at a final concentration of 20 μM, corresponding to 8 mg (40 kDa), 30 mg (150 kDa), and 50 mg (250 kDa) per 10 mL of precursor. The mixtures were cast into identical acrylic molds. All molds were placed on a 60 °C hot plate for 2 h to ensure complete gelation. The resulting hydrogels were sealed in airtight containers and stored at 4 °C until use.

Characterization of hydrogel swelling

To investigate the evolution of the mesh size of the PAAm hydrogel during swelling, we monitored changes in its macroscopic dimensions over time and correlated them with the underlying network structure. A hydrogel sample (2 cm × 2 cm × 1.5 mm), prepared as described above, was immersed in 20 mL of deionized (DI) water and allowed to swell freely at room temperature. During the swelling process, the linear dimension of the hydrogel was periodically measured. After approximately 18 h, the sample exhibited negligible dimensional changes, and measurements were continued up to 22 h to confirm that equilibrium swelling had been reached.

Characterization of FITC diffusion in hydrogel via fluorescence recovery after photobleaching (FRAP)

The synthesized hydrogel samples containing encapsulated FITC molecules were first immersed in an identical FITC solution for free swelling to prevent FITC loss. Swelling was monitored, and once samples reached the desired size, they were removed, sealed in airtight bags, and stored at 4 °C for preservation.

FRAP measurements were performed using a confocal laser scanning microscope equipped with a 20 × objective and a 488 nm laser (10 mW). A hydrogel sample (10 mm × 10 mm × 1.5–3 mm) was mounted on the microscope stage. A circular region (25 μm diameter) at the center of the hydrogel was photobleached by focusing the laser at full power for 4 s. Fluorescence recovery was monitored at 1-second intervals for 100 s using the 488 nm scanning laser operated at 0.5% of its maximum power. System calibration was performed prior to imaging to ensure optimal resolution and focus.

To extract diffusivity parameters, the normalized intensity recovery curves were fitted using the Soumpasis equation [29], which models diffusion-driven recovery dynamics. The normalized intensity $\bar{I}(t)$ is defined as:

$$\bar{I}(t) = \frac{I(t) - I(0)}{I(\infty) - I(0)} \tag{A.1}$$

where $I(t)$ is the fluorescence intensity is measured at time t, $I(0)$ is the intensity immediately after bleaching, and $I(\infty)$ is the plateau intensity representing complete recovery. The theoretical model [36] used for fitting is:

$$\bar{I}(t) = e^{-\omega^2/2Dt}\left[B_0\left(\frac{\omega^2}{2D}\right)^2 + B_1\left(\frac{\omega^2}{2D}\right)\right] \tag{A.2}$$

where ω is the radius of the bleached spot, D is the molecule diffusivity, and B_0 and B_1 are the modified Bessel functions of the first kind of order 0 and 1, respectively. The fitting procedure minimizes the mean square error between the experimental data and the model, allowing for accurate determination of the molecule diffusivity, D.

For each condition, two independent hydrogel samples were tested. For each hydrogel, three bleaching locations were analyzed and averaged to obtain a representative diffusivity value. Error bars represent the standard deviation calculated from independent hydrogel samples.

Quantitative analysis of FITC-dextran diffusion in DI water

The fluorescence intensity of FITC was calibrated using a Qubit 4 Fluorometer. For release experiments, FITC-encapsulated hydrogel samples (2 cm × 2 cm × 1.5 mm; ~0.6 mL of hydrogel precursor) were immersed in 20 mL of DI water to permit free swelling and diffusion. At designated time points, 200 μL of the surrounding DI water was collected for fluorescence measurement and then returned to the container to maintain a constant volume. Throughout the experiment, the container was sealed with Parafilm and wrapped in aluminum foil to minimize evaporation and prevent light exposure.

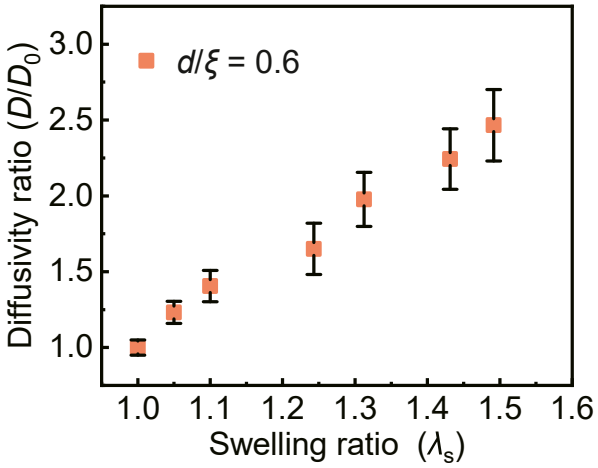


Fig. A1. Normalized diffusivity ratio of 40 kDa FITC (d/ξ = 0.6) in hydrogels with different swelling ratios. All values represent mean ± SD (n = 6, three bleached spots per gel, two independently prepared hydrogels)

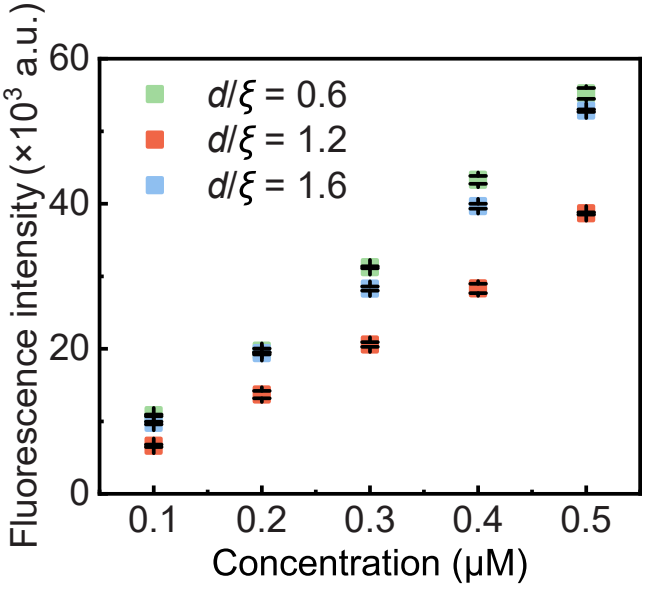


Fig. A2. Fluorescence calibration for FITC–dextran. Calibration curves of fluorescence intensity as a function of FITC–dextran concentration for 40 kDa (d/ξ = 0.6), 150 kDa (d/ξ = 1.2), and 250 kDa (d/ξ = 1.6) species. Values represent mean ± SD (n = 3)

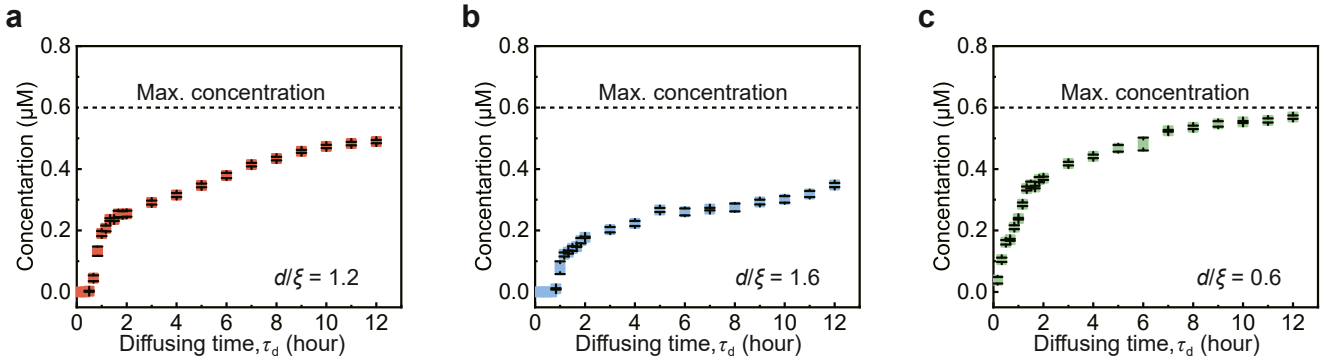


Fig. A3. Comprehensive FITC release profile. (**a**) 150 kDa FITC–dextran (d/ξ =1.2) (**b**) 250 kDa FITC–dextran (d/ξ =1.6), and (**c**) 40 kDa FITC–dextran (d/ξ =0.6). All values represent mean ± SD (n = 3)

Appendix B. Size estimation of fluorescein isothiocyanate (FITC) molecule

Three different sizes of FITC were used, with molecular weights of 40 kDa, 150 kDa, and 250 kDa. Their corresponding hydrodynamic diameters (in nanometers) were estimated following an empirical formula [37]:

$$d \approx 0.408 M_w^{0.5} \tag{B.1}$$

where d is the hydrodynamic diameter of the FITC-dextran molecules expressed in angstrom, and M_w is the weight-average molecular weight expressed in Da. The hydrodynamic diameters of FITC with molecular weights of 40 kDa, 150 kDa, and 250 kDa were estimated to be approximately 8.16 nm, 15.8 nm, and 20.4 nm, respectively. Their corresponding ratios of d/ξ were approximately 0.6, 1.2, and 1.6, respectively.

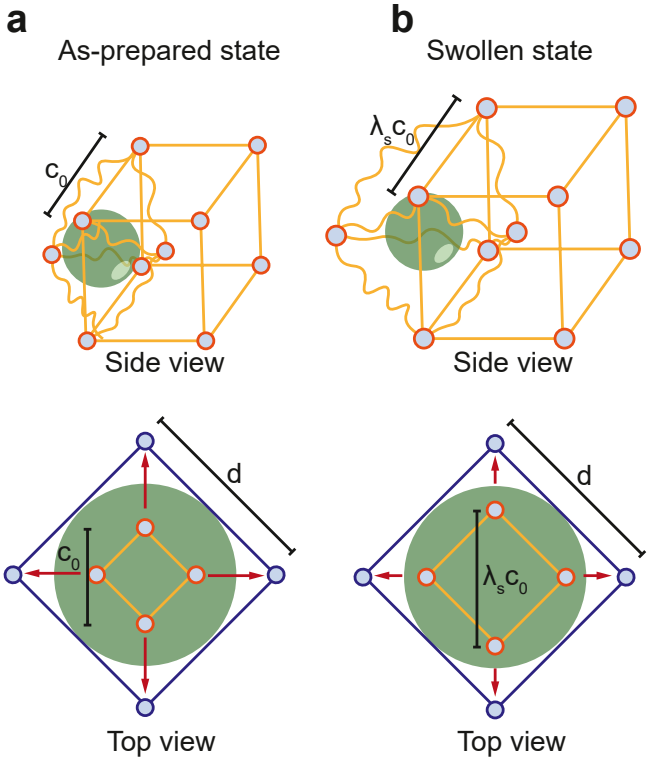


Fig. B1. Schematic of molecular penetration through a polymer cage. Side and top views are shown for (**a**) the as–prepared state and (**b**) the swollen state

Data availability

Data will be made available on request.

References

[1] S.J. Buwalda, T. Vermonden, W.E. Hennink, Hydrogels for therapeutic delivery: current developments and future directions, Biomacromolecules 18 (2) (2017) 316–330.
[2] S.W. Kim, Y.H. Bae, T. Okano, Hydrogels: swelling, drug loading, and release, Pharm. Res. 9 (3) (1992) 283–290.
[3] B. Li, et al., Combinatorial design of nanoparticles for pulmonary mRNA delivery and genome editing, Nat. Biotechnol. 41 (10) (2023) 1410–1415.
[4] B. Li, et al., The potential of biomimetic nanoparticles for tumor-targeted drug delivery, Nanomedicine 13 (16) (2018) 2099–2118.
[5] B. Li, et al., Accelerating ionizable lipid discovery for mRNA delivery using machine learning and combinatorial chemistry, Nat. Mater. 23 (7) (2024) 1002–1008.
[6] P. Vega-Vásquez, N.S. Mosier, J. Irudayaraj, Nanoscale drug delivery systems: from medicine to agriculture, Front. Bioeng. Biotechnol. 8 (2020) 79.
[7] M. Li, et al., Recent advances in nanoparticle-mediated co-delivery system: a promising strategy in medical and Agricultural Field, Int. J. Mol. Sci. 24 (6) (2023) 5121.
[8] D. Lombardo, et al., Soft interaction in liposome nanocarriers for therapeutic drug delivery, Nanomaterials 6 (7) (2016) 125.
[9] Y. Yang, et al., Smart materials for drug delivery and cancer therapy, View 2 (2) (2021) 20200042.
[10] Y.J. Yang, et al., Tuning selective transport of biomolecules through site-mutated nucleoporin-like protein (nlp) hydrogels, Biomacromolecules 22 (2) (2021) 289–298.
[11] Y.J. Yang, et al., Nucleopore-inspired polymer hydrogels for selective biomolecular transport, Biomacromolecules 19 (10) (2018) 3905–3916.
[12] T.H. Wong, et al., Tissue-adhesive hydrogel–MXene biosensor for in situ intraoral TNF-α detection, Sci. Adv. 12 (3) (2026) eady9180.
[13] K. Saalwächter, S. Seiffert, Dynamics-based assessment of nanoscopic polymer-network mesh structures and their defects, Soft Matter 14 (11) (2018) 1976–1991.
[14] P.F. Green, E.J. Kramer, Matrix effects on the diffusion of long polymer chains, Macromolecules 19 (4) (1986) 1108–1114.
[15] L.M. Weber, C.G. Lopez, K.S. Anseth, Effects of PEG hydrogel crosslinking density on protein diffusion and encapsulated islet survival and function, J. Biomed. Mater. Res. Part A 90 (3) (2009) 720–729.
[16] S. Candau, J. Bastide, M. Delsanti, Structural, elastic, and dynamic properties of swollen polymer networks, Polym. Netw. (2005) 27–71.
[17] E.P. Jonášová, B.T. Stokke, V. Prot, Interrelation between swelling, mechanical constraints and reaction–diffusion processes in molecular responsive hydrogels, Soft Matter 18 (7) (2022) 1510–1524.
[18] J. Siepmann, N.A. Peppas, Higuchi equation: derivation, applications, use and misuse, Int. J. Pharm. 418 (1) (2011) 6–12.
[19] D. Paul, Elaborations on the Higuchi model for drug delivery, Int. J. Pharm. 418 (1) (2011) 13–17.
[20] P.L. Ritger, N.A. Peppas, A simple equation for description of solute release I. Fickian and non-fickian release from non-swellable devices in the form of slabs, spheres, cylinders or discs, J. Control. Release 5 (1) (1987) 23–36.
[21] P.L. Ritger, N.A. Peppas, A simple equation for description of solute release II. Fickian and anomalous release from swellable devices, J. Control. Release 5 (1) (1987) 37–42.

[22] I.Y. Wu, et al., Interpreting non-linear drug diffusion data: utilizing Korsmeyer-Peppas model to study drug release from liposomes, Eur. J. Pharm. Sci. 138 (2019) 105026.
[23] J. Siepmann, N.A. Peppas, Modeling of drug release from delivery systems based on hydroxypropyl methylcellulose (HPMC), Adv. Drug Deliv. Rev. 64 (2012) 163–174.
[24] F. Babayekhorasani, et al., Nanoparticle diffusion in crowded and confined media, Soft Matter 12 (40) (2016) 8407–8416.
[25] J.D.C. Jacob, et al., Diffusive dynamics of nanoparticles in ultra-confined media, Soft Matter 11 (38) (2015) 7515–7524.
[26] A.H. Slim, R. Poling-Skutvik, J.C. Conrad, Local confinement controls diffusive nanoparticle dynamics in semidilute polyelectrolyte solutions, Langmuir 36 (31) (2020) 9153–9159.
[27] L.-H. Cai, S. Panyukov, M. Rubinstein, Hopping diffusion of nanoparticles in polymer matrices, Macromolecules 48 (3) (2015) 847–862.
[28] J. Liu, S. Lin, Strain-engineered particle diffusion in uniaxially deformed polymer networks, J. Mech. Phys. Solids 191 (2024) 105732.
[29] D. Soumpasis, Theoretical analysis of fluorescence photobleaching recovery experiments, Biophys. J. 41 (1) (1983) 95–97.
[30] C. Ye, et al., Mechano-diffusion of particles in stretchable hydrogels, Soft Matter 21 (12) (2025) 2230–2241.
[31] B. Amsden, An obstruction-scaling model for diffusion in homogeneous hydrogels, Macromolecules 32 (3) (1999) 874–879.
[32] E.M. Arruda, M.C. Boyce, A three-dimensional constitutive model for the large stretch behavior of rubber elastic materials, J. Mech. Phys. Solids 41 (2) (1993) 389–412.
[33] S. Ramakrishna, et al., Stratified polymer grafts: synthesis and characterization of layered 'brush'and 'gel'structures, Adv. Mater. Interfaces 1 (2014).
[34] X. Zhao, A theory for large deformation and damage of interpenetrating polymer networks, J. Mech. Phys. Solids 60 (2) (2012) 319–332.
[35] W. Hong, et al., A theory of coupled diffusion and large deformation in polymeric gels, J. Mech. Phys. Solids 56 (5) (2008) 1779–1793.
[36] P.J. Bickel, K.A. Doksum. Mathematical Statistics: Basic Ideas and Selected Topics, Volumes I-ii Package, Chapman and Hall/CRC, 2015.
[37] B.G. Amsden, Hydrogel mesh size and its impact on predictions of mathematical models of the solute diffusion coefficient, Macromolecules 55 (18) (2022) 8399–8408.